Pyrite/H$_2$O$_2$/hydroxylamine system for efficient decolorization of rhodamine B

Guang-Jun He, Deng-Jie Zhong, Yun-Lan Xu, Peng Liu, Si-Jing Zeng and Shuang Wang

ABSTRACT

To improve the efficiency of the Fe(II)/Fe(III) cycle and continuous reactivity of pyrite, a pyrite/H$_2$O$_2$/hydroxylamine (HA) system was proposed to treat rhodamine B (RhB). The results showed that near-complete decolorization and 52.8% mineralization 50 mg L^{-1} RhB were achieved under its optimum conditions: HA 0.8 mM, H$_2$O$_2$ 1.6 mM, pyrite 0.4 g L^{-1}, and initial pH 4.0. The degradation reaction was dominated by an •OH radical produced by the reaction of Fe^{2+} with H$_2$O$_2$ in solution. HA primarily had two roles: in solution, HA could accelerate the Fe(II)/Fe(III) cycle through its strong reducibility to enhance RhB decolorization; on the pyrite surface, HA could improve the continuous reactivity of pyrite by inhibiting the oxidation of pyrite. In addition, the dosing manner of HA had a significant effect on RhB decolorization. In addition, the high decolorization and mineralization efficiency of other dye pollutants suggested that the pyrite/H$_2$O$_2$/HA system might be widely used in textile wastewater treatment.

Key words | H$_2$O$_2$, hydroxylamine, hydroxyl radical, pyrite (FeS$_2$), rhodamine B

Guang-Jun He
Deng-Jie Zhong (corresponding author)
Yun-Lan Xu
Peng Liu
Si-Jing Zeng
Shuang Wang
School of Chemical Engineering,
Chongqing University of Technology,
Chongqing 400054,
China
E-mail: djzhong@cqut.edu.cn

HIGHLIGHTS

- A pyrite/H$_2$O$_2$/HA system was proposed for efficient RhB decolorization in a wide-range pH of 3.0–10.0.
- HA could not only promote the Fe(II)/Fe(III) cycle to enhance the decolorization of RhB, but also improve the continuous reactivity of pyrite.
- The dosing manner of HA had a notable effect on RhB decolorization.
- Complete decolorization and high mineralization of other dye pollutants were achieved by the proposed system.
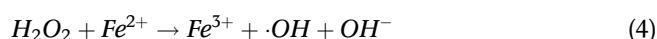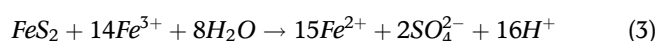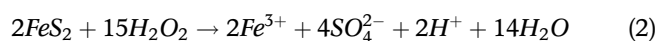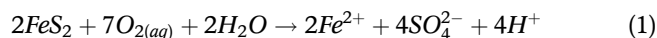
GRAPHICAL ABSTRACT
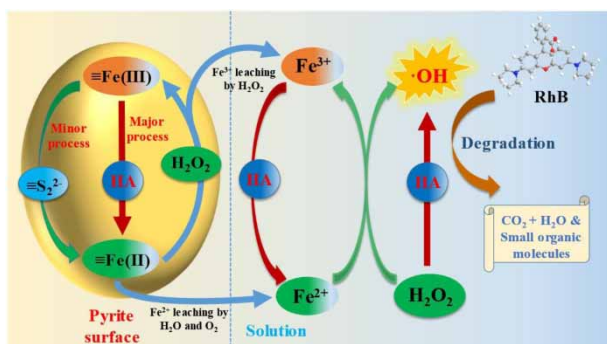
INTRODUCTION

Dye effluent released from textile industries is toxic and carcinogenic, which can cause a severe impact on human health and water ecosystems (Brillas & Martínez-Huitle 2015; Banazadeh *et al.* 2016; Javaid & Qazi 2019). Even low concentrations ($<1.0 \text{ mg L}^{-1}$) of dye can cause adverse effects in water (Javaid & Qazi 2019). Many nations have rigorous regulations on the discharge of textile industry wastewater, which must be properly treated to eliminate the excessive concentrations of chroma and chemical oxygen demand (COD) (Mahalingam *et al.* 2017). Therefore, there is a strong demand for efficient and advanced treatment technologies. Among the existing wastewater treatment technologies, advanced oxidation processes (AOPs) have attracted the attention of many researchers, because AOPs can convert most organic pollutants into smaller compounds or even CO_2 due to the highly effective reactive oxygen species (ROS) produced during the reaction process (Bagal & Gogate 2014; Zhu *et al.* 2019; Sun *et al.* 2021).

The Fenton process is one of the most widely used AOPs because of its high oxidation performance, simple operation, and environmental friendliness (Wang *et al.* 2016). However, there are still some drawbacks, such as a narrow working pH range (2.5–4.0), a large amount of iron sludge, and difficulty in recovering homogeneous catalysts (Fe^{2+}) (Yuan *et al.* 2013; Luo *et al.* 2019). In order to overcome these short-comings, iron-based mineral heterogeneous Fenton-like processes for wastewater treatment have been broadly studied due to their high performance, non-toxicity, and cheapness (Chen *et al.* 2015a; Zhao *et al.* 2020; Zhou *et al.* 2020; Zhu *et al.* 2020). Among the iron-based minerals, pyrite (FeS_2) is a highly reactive, abundant mineral found in the Earth's crust (Gu *et al.* 2020). Pyrite can release

enormous Fe^{2+} via Equations (1)–(3) in the pyrite/H₂O₂ system, and then many ·OH can be produced via Equation (4) to degrade organic pollutants (Ye *et al.* 2018). In addition, large amounts of H^+ are released through Equations (1)–(3) to provide a low pH value, which is beneficial to the Fenton reaction shown in Equation (4) (Zhu *et al.* 2020). Moreover, disulfide (S_2^{2-}) can act as an electron donor as in Equation (3) on pyrite surfaces to accelerate the Fe(II)/Fe(III) cycle, which is the rate-determining step of the Fenton reaction (Zhao *et al.* 2017). Also, it is the rate-determining step of pyrite-based AOPs reported by some researchers (Feng *et al.* 2018; He *et al.* 2021). In addition, the reactivity of pyrite decreases significantly during the repeating experiments with the continuous oxidation of Fe(II) and S_2^{2-} on pyrite surfaces via Equations (1)–(3), which seriously hinders the practical application of the pyrite (Diao *et al.* 2017; Zhou *et al.* 2018). Overall, the above-mentioned defects have significantly influenced further investigations on the degradation performance and application of the pyrite/H₂O₂ system, as well as its development. Therefore, it is of great importance to facilitate the Fe(II)/Fe(III) cycle and improve the continuous reactivity of pyrite for pyrite/H₂O₂ system:

$$2FeS_2 + 7O_{2(aq)} + 2H_2O \rightarrow 2Fe^{2+} + 4SO_4^{2-} + 4H^+ \quad (1)$$

$$2FeS_2 + 15H_2O_2 \rightarrow 2Fe^{3+} + 4SO_4^{2-} + 2H^+ + 14H_2O \quad (2)$$

$$FeS_2 + 14Fe^{3+} + 8H_2O \rightarrow 15Fe^{2+} + 2SO_4^{2-} + 16H^+ \quad (3)$$

$$H_2O_2 + Fe^{2+} \rightarrow Fe^{3+} + \cdot OH + OH^- \quad (4)$$

Hydroxylamine (NH₂OH, HA) is a common reducing agent (Sun *et al.* 2020a). It has been reported that HA can

enhance the Fe(II)/Fe(III) redox cycle in Fenton-like reactions (Chen *et al.* 2011; Zou *et al.* 2013; Hou *et al.* 2017). In addition, in the pre-experiments, we found that HA could improve the continuous reactivity of pyrite. However, this role of HA has rarely been systematically studied to the best of our knowledge. Moreover, although HA is toxic, it can be rapidly decomposed into non-toxic inorganic substances, such as NO_2^-, N_2O, and N_2, in Fenton-like processes (Chen *et al.* 2011; Zou *et al.* 2013; Li *et al.* 2019a). Therefore, HA was selected in this work to develop the dyes decolorization ability of pyrite/H₂O₂ system by boosting the Fe(II)/Fe(III) cycle and improving the continuous reactivity of pyrite. To best of our knowledge, there have been few comprehensive studies on the degradation of organic dye pollutants by pyrite/H₂O₂/HA systems.

In this study, the pyrite/H₂O₂/HA system was proposed to decolorize rhodamine B (RhB, an essential example of xanthene dyes (Diao *et al.* 2017)). The main objectives were to: (i) evaluate the feasibility of pyrite/H₂O₂/HA system for RhB decolorization; (ii) explore the influencing factors including HA concentration, H₂O₂ concentration, pyrite dosage, RhB concentration, and initial pH; (iii) reveal the mechanism of RhB decolorization by the pyrite/H₂O₂/HA system; and (iv) investigate the influence of HA dosing manners, and degradation performance of pyrite/H₂O₂/HA system to other dye pollutants.

MATERIALS AND METHODS

Materials

Hydrogen peroxide (H₂O₂, 30 wt.%), RhB, orange II (OR), methyl orange (MO), neutral red (NR), hydroxylamine hydrochloride (NH₂OH·HCl, HA·HCl), ferrous sulfate heptahydrate (FeSO₄·7H₂O), *tert*-butyl alcohol (TBA), sodium hydroxide (NaOH), ethanol (EtOH), hydrochloric acid (HCl), titanic sulfate (Ti(SO₄)₂), and sulfuric acid (H₂SO₄) were acquired from Chengdu Kelong chemical reagent factory (Chengdu, China). 8-Hydroxyquinoline, methylene blue (MB), sodium thiosulfate pentahydrate (Na₂S₂O₃·5H₂O), sodium acetate trihydrate (CH₃COONa·3H₂O), potassium dihydrogen phosphate (KH₂PO₄), 1,10-phenanthroline, and sodium carbonate (Na₂CO₃) were bought from Xilong Science Co., Ltd (Shantou, China). All the reagents were of analytical grade and utilized as obtained without further purification. Deionized water was used in all experiments. Pyrite samples were bought from Wanbao Mining Co., Ltd (Beijing, China). After the sample was ground, it was immersed in 0.1 M HCl

to keep its purity of the surface. Then the sample was washed with EtOH and deionized water, and latterly placed in a vacuum drying oven (DZF-6021, Shanghai, China) at 60 °C until it was dry. Finally, it was kept in a closed glass bottle to avoid oxidation.

Experimental procedures

Batch experiments of RhB decolorization were carried out in a 100 mL flat-bottom beaker containing about 100 mL reaction solution. The beaker was placed on a magnetic stirrer with constantly stirring by a magnetic stir bar at room temperature (25 ± 2 °C). A stock solution of HA (40 mM; prepared daily) or RhB (1.0 g L⁻¹) was stored in a 100 mL volumetric flask and kept in a dark cabinet to prevent photochemical reactions. For a typical test procedure, preset volumes of RhB and HA from the stock solution were poured into the beaker, and next the initial pH was adjusted to a predetermined value with diluted NaOH and H₂SO₄. Then, a specific dose of pyrite and a certain volume of 30 wt.% H₂O₂ were added into the reaction solution to trigger the oxidation reaction. At the preset interval, 1.0 mL reaction suspension was sampled and quenched by 1.0 mL EtOH. Then, the suspension was filtered through a 0.22 μm membrane filter for further analysis. To test the continuous reactivity of pyrite, the pyrite was separated from the solution by centrifugation at 4,000 rpm (TDL-5A, Changzhou, China) after 30 min reaction time, and then washed with EtOH, and lastly dried in the vacuum drying oven at 60 °C for 8 h. The recycled pyrite was reused by adding the same amounts of RhB, HA, and H₂O₂. Unless otherwise specified, $[RhB]_0 = 50$ mg L⁻¹, $[pyrite]_0 = 0.4$ g L⁻¹, $[HA]_0 = 0.8$ mM, $[H_2O_2]_0 = 1.6$ mM, and initial pH = 4.0. All experiments were conducted in duplicate and the data were averaged. The error bars in the figures represent the standard deviation.

Analysis and characterization

The decolorization efficiency of RhB, MO, OR, MB, or NR was calculated by Equation (5):

$$Decolorization\ efficiency\ (\%) = \frac{A_0 - A_t}{A_0} \times 100\% \tag{5}$$

where A_0 and A_t is the absorbance of the reaction solution at time 0 and t, respectively. The absorbance of RhB, MO, OR, MB, or NR solution was tested using a UV-vis spectrophotometer (UV-6100S, MRTASH, Shanghai, China) at the maximum absorption wavelengths of 554, 436, 486, 659, or

541 nm, respectively. The concentration of dissolved ferrous (Fe^{2+}) was confirmed by the 1,10-phenanthroline method with the UV-vis spectrophotometer at a wavelength of 510 nm, and the concentration of total dissolved iron (Fe_{total}) was confirmed following the addition of HA (Hou *et al.* 2017). The mutual interference of Fe^{2+}, Fe^{3+} and RhB solutions in spectrophotometric analysis was investigated based on their colors. The results are shown in Figure S1 (supplementary information). The results in Figure S1a show that the influence of Fe^{3+} on the determination of Fe Fe^{2+} is negligible, but RhB interferes with the determination of Fe^{2+} and Fe^{3+}, and the degree of interference increases with the increase in RhB concentration. Therefore, the concentrations of Fe^{2+} and Fe_{total} can only be measured without RhB in the solution. In addition, the presence of Fe^{2+} and Fe^{3+} hardly affected the determination of RhB (Figure S1b). The concentration of H_2O_2 was analyzed using the titanate method at 405 nm and a UV-vis spectrophotometer (Eisenberg 1943; Luo *et al.* 2019). The HA concentration was determined spectrophotometrically using the 8-hydroxyquinoline method (Frear & Burrell 1955). Total organic carbon (TOC) analysis was implemented by a Shimadzu TOC-L analyzer. In order to avoid the influence of EtOH quencher on the TOC result, it was replaced by 3 mM $Na_2S_2O_3$ to stop the reaction (Li *et al.* 2021). The TOC removal efficiency was computed using Equation (6):

$$TOC \text{ removal efficiency } (\%) = \frac{TOC_0 - TOC_t}{TOC_0} \times 100\% \qquad (6)$$

where TOC_0 and TOC_t is the TOC concentration of the reaction solution at time 0 and t, respectively. The laser particle size analyzer (LPSA, Bettersize2000, China), X-ray diffraction (XRD, SHIMADZU XRD-7000, Japan), and X-ray photo-electron spectrometer (XPS, ThermoFisher K-Alpha, USA) were applied to investigate particle size distribution, crystal structure, and surface products of the pyrite, respectively.

RESULTS AND DISCUSSION

Characterization of pyrite

Figure 1(a) shows the XRD pattern of pyrite. The pattern demonstrates that the diffraction peaks are noted at 2θ of 28.5°, 33.0°, 37.1°, 40.8°, 47.4°, 56.3°, 59.0°, 61.7°, 64.4°, 76.6° and 79.0°, corresponding to the (1 1 1), (2 0 0), (2 1 0), (2 1 1), (2 2 0), (3 1 1), (2 2 2), (2 3 0), (3 2 1), (3 3 1) and (4 2 0) characteristic planes of FeS_2 (JCPDS card no. 42-1340), respectively. The results indicated that pyrite has a good crystallized phase and cubic structure. The particle size distribution graph of pyrite is presented in Figure 1(b), and its size was macroscopically mainly distributed in the range 2–50 μm.

Feasibility of RhB decolorization by the pyrite/H₂O₂/HA system

Figure 2 shows the RhB decolorization efficiency of pyrite, H_2O_2, HA, pyrite/H_2O_2, pyrite/HA, H_2O_2/HA, and the pyrite/H_2O_2/HA system. The results unveiled that RhB is barely decolorized by pyrite, H_2O_2, HA or pyrite/HA within 30 min treatment, demonstrating that the reactions of RhB with pyrite, H_2O_2, HA or pyrite/HA are negligible.
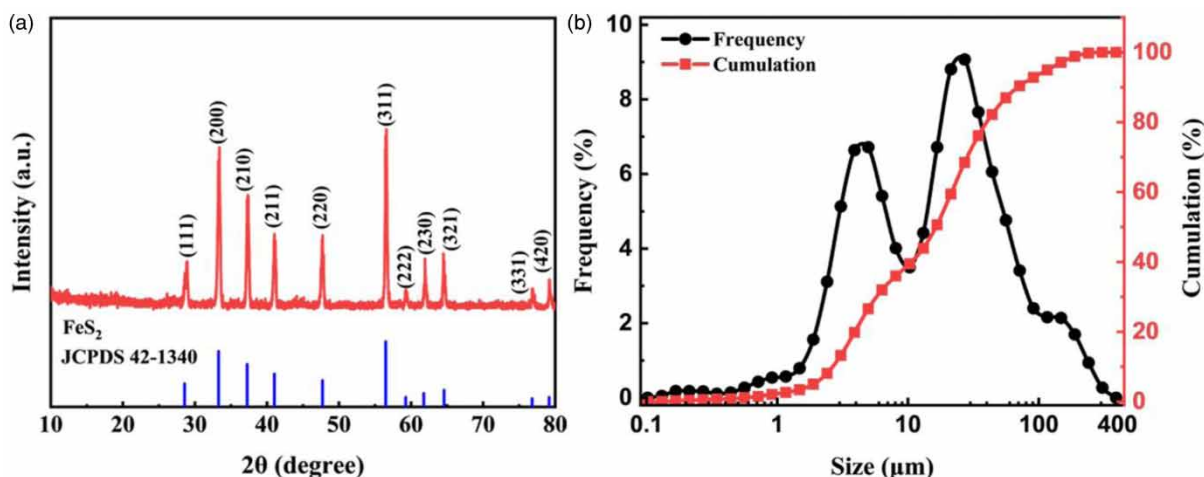

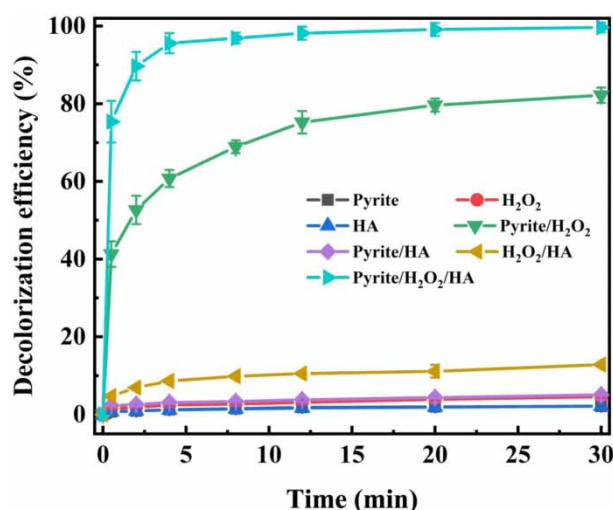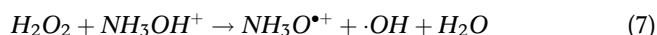**Figure 1** │ (a) XRD pattern and (b) particle size distribution graph of pyrite.

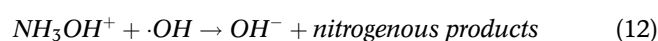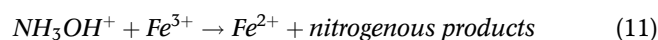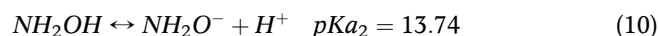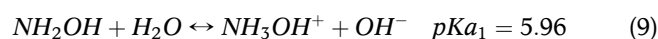**Figure 2** | RhB decolorization efficiency of different systems.

Nearly 13% of RhB was removed by the H_2O_2/HA system, which is because H_2O_2 can be activated by HA to generate radicals via Equations (7) and (8) (Chen et al. 2015b; Wang et al. 2018). In the pyrite/H_2O_2 system, the decolorization efficiency of RhB was around 82%, which was mainly attributed to the generation of ·OH via the reaction between H_2O_2 and Fe^{2+} (Equation (4)) (Zhu et al. 2020). Importantly, the pyrite/H_2O_2/HA system obtained the highest RhB decolorization efficiency (99.6%), which is nearly 20% higher than that of the pyrite/H_2O_2 system. The results indicated that the added HA hastens the Fe(III)/Fe(II) cycle and then boosts the H_2O_2 decomposition to produce more ·OH radicals for RhB decolorization. In order to further examine the feasibility of the pyrite/H_2O_2/HA system, TOC removal efficiency of different systems was also measured (Figure S2a). Within 30 min, about 1.8%, 2.6%, 0.7%, 7.9%, 2.4%, 38.5%, and 52.8% of RhB are mineralized by pyrite, H_2O_2, HA, H_2O_2/HA, pyrite/HA, pyrite/H_2O_2 and pyrite/H_2O_2/HA systems, respectively. The mineralization efficiency of RhB by the pyrite/H_2O_2/HA system is significantly higher than that of the other six systems, demonstrating that it is feasible and displays outstanding performance:

$$H_2O_2 + NH_3OH^+ \rightarrow NH_3O^{\bullet +} + \cdot OH + H_2O \tag{7}$$

$$H_2O_2 + NH_3O^{\bullet +} \rightarrow NHO + \cdot OH + H_2O + H^+ \tag{8}$$

Effect of HA concentration

Figure 3(a) illustrates the effect of HA concentration on RhB decolorization by the pyrite/H_2O_2/HA system. With the increase in HA concentration, the RhB decolorization

efficiency first increased and then remained stable. In detail, when the HA concentration was increased from 0.0 to 0.8 mM, the decolorization efficiency of RhB increased from 81.2% to 99.6%, but the decolorization efficiency slightly decreased to 97.2% as the concentration of HA further increased to 1.2 mM. Since the main existing form of HA changes with the change of pH according to Equations (9) and (10) (Robinson & Bower 1961; Hughes et al. 1971), the variation of solution pH with different HA concentrations was checked (Figure S2b). This showed that the solution pH ranges from 3.0 to 4.0 in the presence of both 0.2 mM and 1.2 mM HA with other parameters were identical in the pyrite/H_2O_2/HA system. The results demonstrated that NH_3OH^+ is the main existing form of HA as calculated by Equation (9). Therefore, the NH_3OH^+ concentration regulates the process of RhB decolorization. The Fe(II)/Fe(III) cycle can be accelerated with an increase in NH_3OH^+ concentration through Equation (11) (Zou et al. 2013) and thereby improving the generation rate of ·OH, but excess NH_3OH^+ had a scavenging effect on ·OH via Equation (12) with $k < 5.0 \times 10^8$ M^{-1} s^{-1} (He et al. 2020). Therefore, 0.8 mM was selected as the optimal concentration of HA:

$$NH_2OH + H_2O \leftrightarrow NH_3OH^+ + OH^- \quad pKa_1 = 5.96 \tag{9}$$

$$NH_2OH \leftrightarrow NH_2O^- + H^+ \quad pKa_2 = 13.74 \tag{10}$$

$$NH_3OH^+ + Fe^{3+} \rightarrow Fe^{2+} + nitrogenous\ products \tag{11}$$

$$NH_3OH^+ + \cdot OH \rightarrow OH^- + nitrogenous\ products \tag{12}$$

Effect of H_2O_2 concentration

Figure 3(b) shows the effect of H_2O_2 concentration on RhB decolorization by the pyrite/H_2O_2/HA system. The results show that the decolorization efficiency of RhB first increased and later remained steady with the increase in H_2O_2 concentration. Specifically, when the H_2O_2 concentration was increased from 0.4 to 1.6 mM, the decolorization efficiency of RhB increased from 64.2% to 99.6%. While the decolorization efficiency slightly reduced to 97.4% with the H_2O_2 concentration further increases to 2.0 mM. This is because when the concentration of H_2O_2 is at a low level, the amount of generated ·OH increases with the increase in H_2O_2 concentration, which increases the decolorization efficiency of RhB. However, when the concentration of H_2O_2 is at a high level, excess H_2O_2 can quickly react with the high active radicals ·OH to form low active radicals $HO_2\cdot$ according to Equation (13) (Bae
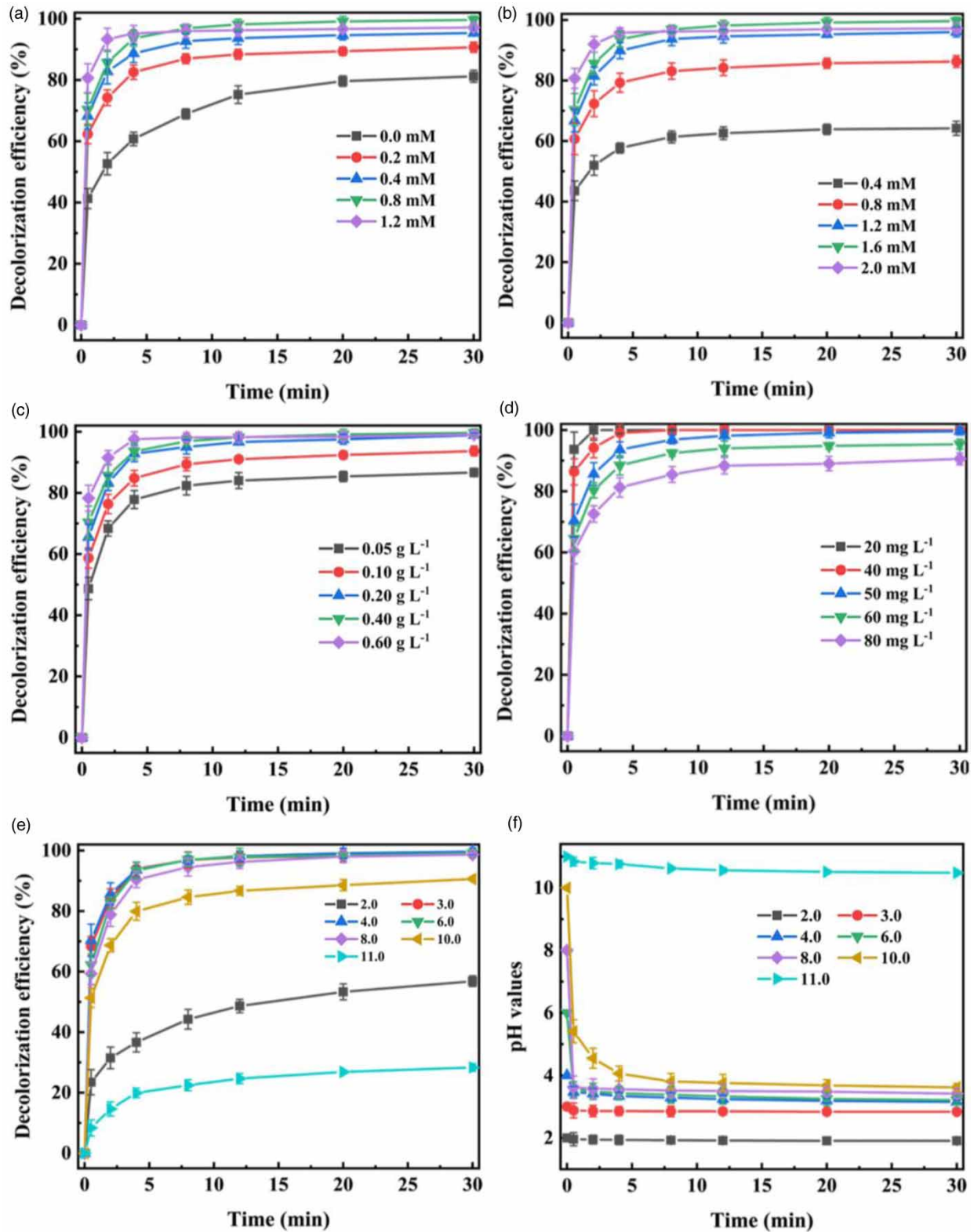
Figure 3 | Effect of (a) HA concentration, (b) H$_2$O$_2$ concentration, (c) pyrite dosage, (d) RhB concentration and (e) initial pH on RhB decolorization efficiency, and (f) variation of solution pH during the reaction time with different initial pH.

et al. 2013; Zhang *et al.* 2014; Sun *et al.* 2020b), which makes the decolorization efficiency basically stable. Therefore, 1.6 mM was chosen as the optimal concentration of H$_2$O$_2$:

$$H_2O_2 + {}^\bullet OH \rightarrow HO_2^\bullet + H_2O \tag{13}$$

Effect of pyrite dosage

Figure 3(c) presents the effect of pyrite dosage on RhB decolorization by the pyrite/H$_2$O$_2$/HA system. Like the effect of H$_2$O$_2$ and HA, the RhB decolorization efficiency initially increased and then remained stable with the increase in pyrite dosage. This is because the amount of Fe^{2+} dissolved from pyrite continuously rises with the increase in pyrite dosage (Bae *et al.* 2013; Oral & Kantar 2019), leading to more •OH generated in solution to decolorize RhB. However, redundant Fe^{2+} can quench •OH via Equation (14) with k = $(1.7–4.5) \times 10^7$ M^{-1}s^{-1} (Zhu *et al.* 2019), thus making the decolorization efficiency remain stable. Since the solution pH may change with the increase of pyrite dosage via Equations (1)–(3), and then influence the RhB decolorization efficiency, the variation of solution pH with different pyrite dosages (0.05, 0.1 or 0.6 g L^{-1}) was measured (Figure S2c). The results illustrated that the variation in solution pH with different pyrite dosages was similar, indicating that the effect of pH change on RhB decolorization was negligible. The result (Figure 3(c)) shows that 0.4 g L^{-1} is the optimal pyrite dosage:

$$Fe^{2+} + {}^\bullet OH \rightarrow Fe^{3+} + OH^- \tag{14}$$

Effect of RhB concentration

Figure 3(d) presents the effect of RhB concentration on RhB decolorization by the pyrite/H$_2$O$_2$/HA system. The results display that the decolorization efficiency of RhB drops from 100% to 90.6% with the increase in RhB concentration from 20 to 80 mg L^{-1}. The decrease of decolorization performance is probably attributed to the inadequate generation of radicals for RhB decolorization with constant chemical dosages in the pyrite/H$_2$O$_2$/HA system (Li *et al.* 2019b). Moreover, the number of intermediates produced by the decolorization of RhB will increase with the increase in RhB concentration, which will reduce the chance of RhB decolorization by radicals. Therefore, 50 mg L^{-1} was selected as the suitable RhB concentration in this research for practical and economic considerations.

Effect of initial pH

According to previous studies, the solution pH frequently has a significant impact on organic pollutants degradation in Fenton-like reactions (He *et al.* 2020; Zhao *et al.* 2020; Zhu *et al.* 2020). Here, experiments were performed to investigate the effect of initial pH on RhB decolorization efficiency by the pyrite/H$_2$O$_2$/HA system. As shown in Figure 3(e), the RhB decolorization efficiency was higher than 90% when the initial pH was in the range 3.0–10.0, but it declined significantly when the initial pH was 2.0 (56.8%) or 11.0 (28.4%). To explain the results, the variation of solution pH during the RhB decolorization under different initial pH was examined. The result (Figure 3(f)) shows that the solution pH quickly declined and finally stays in the range 2.5–4.0 (working pH range of Fenton reaction (Luo *et al.* 2019)) when the initial pH is in the range 3.0–10.0, leading to the fast decolorization of RhB. However, the variation of solution pH was negligible under high acidic (initial pH 2.0) and alkaline (initial pH 11.0) conditions due to the strong buffer capacity at extreme pH conditions (Li *et al.* 2021). For initial pH 2.0, the generation of Fe^{2+} was delayed by the reactions of pyrite with dissolved O$_2$ (Equation (1)) and Fe^{3+} (Equation (3)) under these high acidic conditions. Meanwhile, many •OH are consumed by HA (Equation (12)) and Fe^{2+} (Equation (14)). Therefore, the decolorization efficiency of RhB decreased at the initial pH of 2.0. For initial pH 11.0, the low decolorization efficiency of RhB can be explained by the following reasons under this extreme pH condition: (a) the rapid oxidation of the pyrite surface (Todd *et al.* 2003) and the low solubility of Fe^{2+} led to the low concentration of Fe^{2+} in solution, which inhibited the Fenton reaction. (b) NH$_2$OH is the primary form of HA as calculated by Equations (9) and (10) in this pH condition, which has a higher reaction rate (k = 9.5×10^9 M^{-1}s^{-1} (Neta *et al.* 1988)) with •OH than that (k < 5.0×10^8 M^{-1}s^{-1}) of NH$_3$OH$^+$ (the dominant form of HA as pH < 5.96). Thus, more •OH were quenched by NH$_2$OH rather than RhB decolorization. In general, high RhB decolorization efficiency can be achieved at a wide-range pH of 3.0–10.0 by the pyrite/H$_2$O$_2$/HA system, and 4.0 was selected as the optimal initial pH.

Determination of the dominant radicals

According to previous research, EtOH is a common scavenger for both •OH and SO$_4^{\bullet-}$ due to the high reaction constant of EtOH with •OH (k = $(1.2–2.8) \times 10^9$ M^{-1}s^{-1}) and SO$_4^{\bullet-}$ (k = $(1.6–7.7) \times 10^7$ M^{-1}s^{-1}) (Anipsitakis & Dionysiou 2004).

TBA is frequently used as a quenching agent for •OH with a high reaction rate constant of $(3.8–7.6) \times 10^8 \, M^{-1} s^{-1}$ (Anipsitakis & Dionysiou 2004). The concentration of both EtOH and TBA was selected as 800 mM, which corresponds to the molar ratio (500:1) of alcohols to H$_2$O$_2$. This technique has been widely applied by Burrows' research team (Hickerson *et al.* 1998; Stemmler & Burrows 2001). As shown in Figure 4, compared with the decolorization efficiency (99.6%) without scavenger, the decolorization efficiency with EtOH and TBA scavenger decreased to 2.0% and 2.1%, respectively. The results demonstrated that •OH is the dominant radical responsible for RhB decolorization in the pyrite/H$_2$O$_2$/HA system.

Role of HA in RhB decolorization

In order to investigate the role of HA in RhB degradation by the pyrite/H$_2$O$_2$/HA system, the concentration changes of Fe$_{total}$ and Fe^{2+} in solution in pyrite/H$_2$O$_2$ and pyrite/H$_2$O$_2$/HA systems respectively with 800 mM EtOH (to prevent the reaction between Fe^{2+} and •OH via Equation (14)) but without RhB (to exclude the effect of RhB on the determination of Fe^{2+} and Fe$_{total}$ (Figure S1a)) were examined. As exhibited in Figure 5(a), the concentration change of Fe$_{total}$ in solution was almost the same in pyrite/H$_2$O$_2$ and pyrite/H$_2$O$_2$/HA systems, both increasing from about 8.0 mg L^{-1} at 0.5 min to 14.7 mg L^{-1} at 30 min. However, Fe^{2+} concentration in the pyrite/H$_2$O$_2$/HA system was about 3–5 times that of the pyrite/H$_2$O$_2$ system. The results revealed that HA can boost the Fe(II)/Fe(III) cycle in solution and then enhance RhB decolorization. Furthermore,
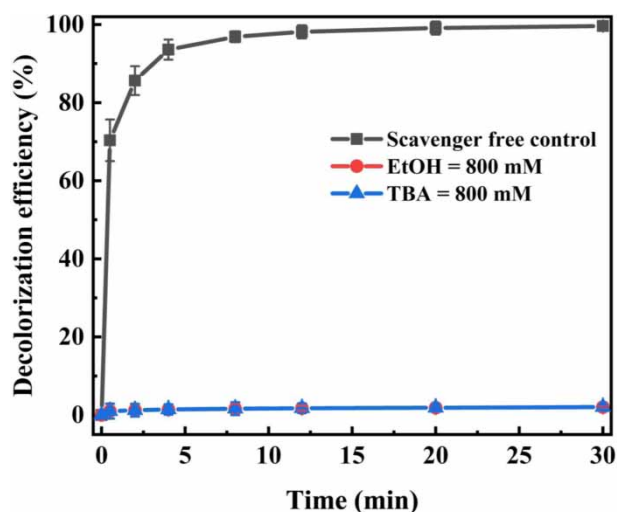

Figure 4 | Quenching experiments of the pyrite/H$_2$O$_2$/HA system.

to further verify the function of HA in the pyrite/H$_2$O$_2$/HA system, the concentration variation of H$_2$O$_2$ in pyrite/H$_2$O$_2$ and pyrite/H$_2$O$_2$/HA systems was compared (Figure 5(b)). This showed that H$_2$O$_2$ was completely decomposed within 12 min in the pyrite/H$_2$O$_2$/HA system. In contrast, the corresponding value was 68% in the pyrite/H$_2$O$_2$ system, suggesting that HA can accelerate the decomposition of H$_2$O$_2$ and thus generate more •OH radicals to improve the decolorization efficiency of RhB. In addition, considering the toxicity of HA, the concentration change of HA in the pyrite/H$_2$O$_2$/HA system was detected. The results (Figure 5(b)) revealed that complete decomposition of HA was achieved in just 8 min, showing the toxicity of HA can be quickly eliminated during the reaction process. Based on these results, the role of HA in the pyrite/H$_2$O$_2$/HA system was that it can accelerate the Fe(II)/Fe(III) cycle via the fast reaction with Fe^{3+} (Equation (11)), and thus enhance the decomposition of H$_2$O$_2$ to produce more •OH radicals, and finally increase RhB decolorization efficiency.

In order to further investigate the role of HA, the iron and sulfur components on pyrite surface before and after reaction in pyrite/H$_2$O$_2$ and pyrite/H$_2$O$_2$/HA systems were detected by XPS (Figure 6). Figure 6(a), 6(c) and 6e show the Fe 2p$_{3/2}$ spectra of pyrite before and after reaction in pyrite/H$_2$O$_2$ and pyrite/H$_2$O$_2$/HA systems, respectively. Three peaks at 707.3, 709.1 and 711.1 eV corresponded to Fe(II)-S, Fe(II)-O and Fe(III)-O species, respectively (Cai *et al.* 2009). The S 2p spectra of pyrite before and after reaction in pyrite/H$_2$O$_2$ and pyrite/H$_2$O$_2$/HA systems are shown in Figure 6(b), 6(d) and 6f, respectively. Three peaks at 162.6, 163.9 and 168.9 eV were attributed to S$_2^{2-}$ (S(-I)), S$_n^{2-}$ (S(0)) and SO$_4^{2-}$ (S(VI)), respectively (Cai *et al.* 2009). The proportions of ferrous iron to total iron (Fe(II)/Fe$_t$) and S(-I) to total sulfur (S(-I)/S$_t$) on pyrite surface were calculated respectively in light of the fitting peak areas of Fe 2p$_{3/2}$ and S 2p core-level spectra (Table S1, supplementary information). For the Fe 2p$_{3/2}$ spectrum of pyrite, the proportion of Fe(II)/Fe$_t$ decreased from 79.63% (before reaction) to 49.94% (after reaction) in the pyrite/H$_2$O$_2$ system due to the oxidation of pyrite via Equations (1)–(3). Surprisingly, the proportion (79.95%) of Fe(II)/Fe$_t$ after the reaction in the pyrite/H$_2$O$_2$/HA system was even slightly higher than that before the reaction because of the reduction of HA. For the S 2p spectrum of pyrite, the proportion of S(-I)/S$_t$ decreased from 52.77% (before reaction) to 36.35% (after reaction) in the pyrite/H$_2$O$_2$ system. While the corresponding value in the pyrite/H$_2$O$_2$/HA system just decreased to 43.74% (after reaction). The results indicate that HA can greatly promote the
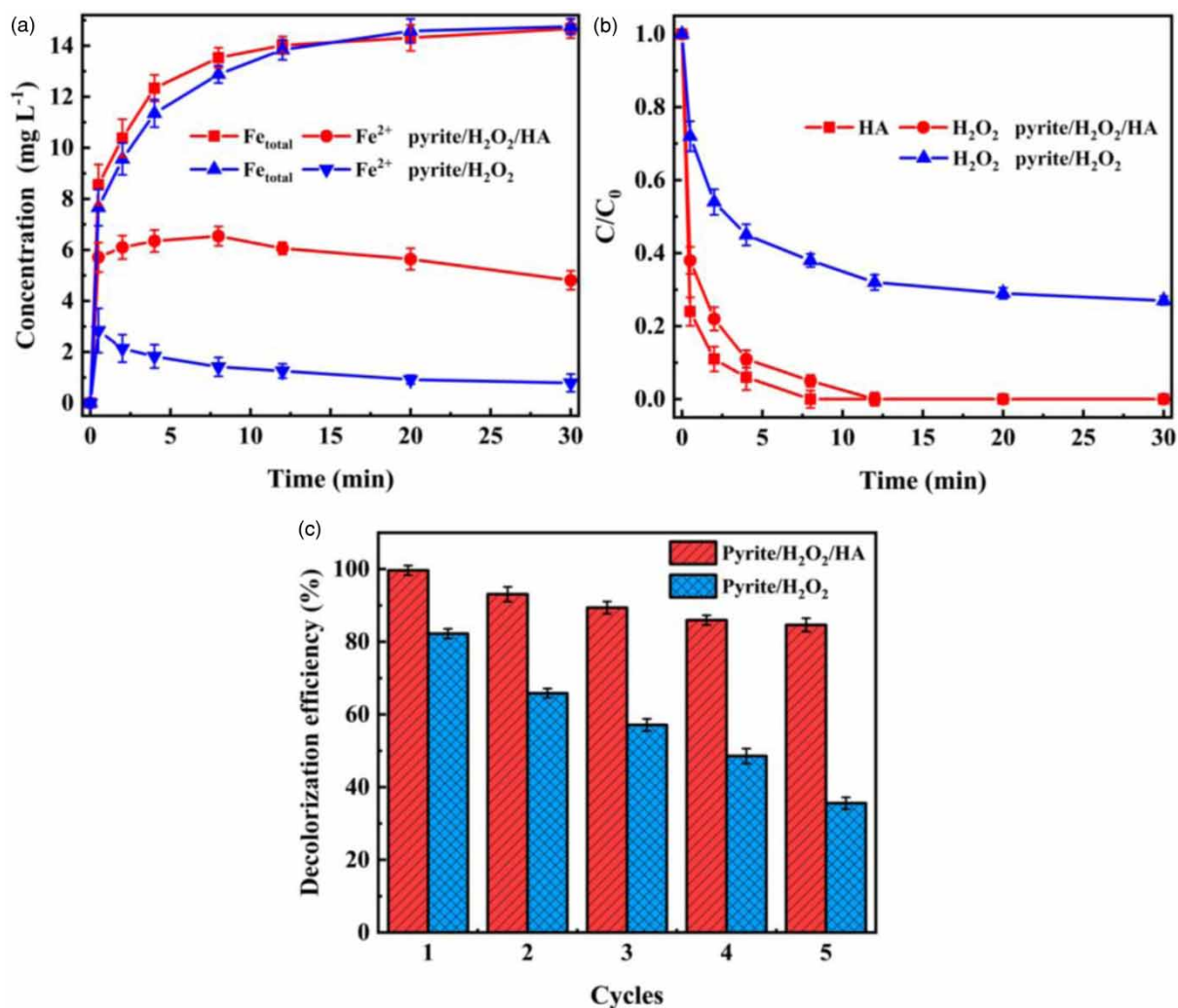
Figure 5 | (a) Concentration variations of Fe_{total} and Fe^{2+} in solution in the pyrite/H_2O_2/HA and pyrite/H_2O_2 systems with 800 mM EtOH but without RhB, (b) concentration changes of HA and H_2O_2 in pyrite/H_2O_2/HA system and H_2O_2 in pyrite/H_2O_2 system, and (c) reusability of pyrite for RhB decolorization in pyrite/H_2O_2/HA and pyrite/H_2O_2 systems.

Fe(II)/Fe(III) cycle on the pyrite surface and inhibit the consumption of S_2^{2-} sites to avoid the oxidation of pyrite. According to previous studies (Diao et al. 2017; Zhou et al. 2018), the oxidation of pyrite will decrease its reuse reactivity. Therefore, the higher continuous reactivity of pyrite may be achieved in the pyrite/H_2O_2/HA system than that of the pyrite/H_2O_2 system. In order to prove this hypothesis, the reuse reactivity of pyrite in pyrite/H_2O_2 and pyrite/H_2O_2/HA systems was investigated. As shown in Figure 5(c), the RhB decolorization efficiency declined by 15.1% in the pyrite/H_2O_2/HA system after five cycles for 30 min treatment, but the corresponding value was 56.7% in the pyrite/H_2O_2 system. The results suggested that pyrite has higher continuous reactivity in the pyrite/H_2O_2/HA system. Therefore, the other role of HA is that it can improve the continuous reactivity of pyrite by inhibiting its oxidation.

Effect of leached iron on RhB decolorization

According to the results in Figure 5(a), the concentration of leached iron in the pyrite/H_2O_2/HA system is high. Therefore, the effect of leached iron on RhB decolorization was investigated. Here, 0.04 g pyrite (0.4 g L^{-1}) was put into a RhB solution, the solution was stirred for 30 min, and then it was filtered. The absorbance of the filtrate was measured as A_0, then HA and H_2O_2 were added to the filtrate. Samples were taken at different times, their absorbance was measured, and their decolorization efficiency was calculated via Equation (5). The results are shown in Figure 7. Nearly 93.0% RhB was decolorized by the leached iron/H_2O_2/HA system, which is just slightly lower than that (99.6%) of the pyrite/H_2O_2/HA system. The results suggested that the leached iron has a dominant effect on
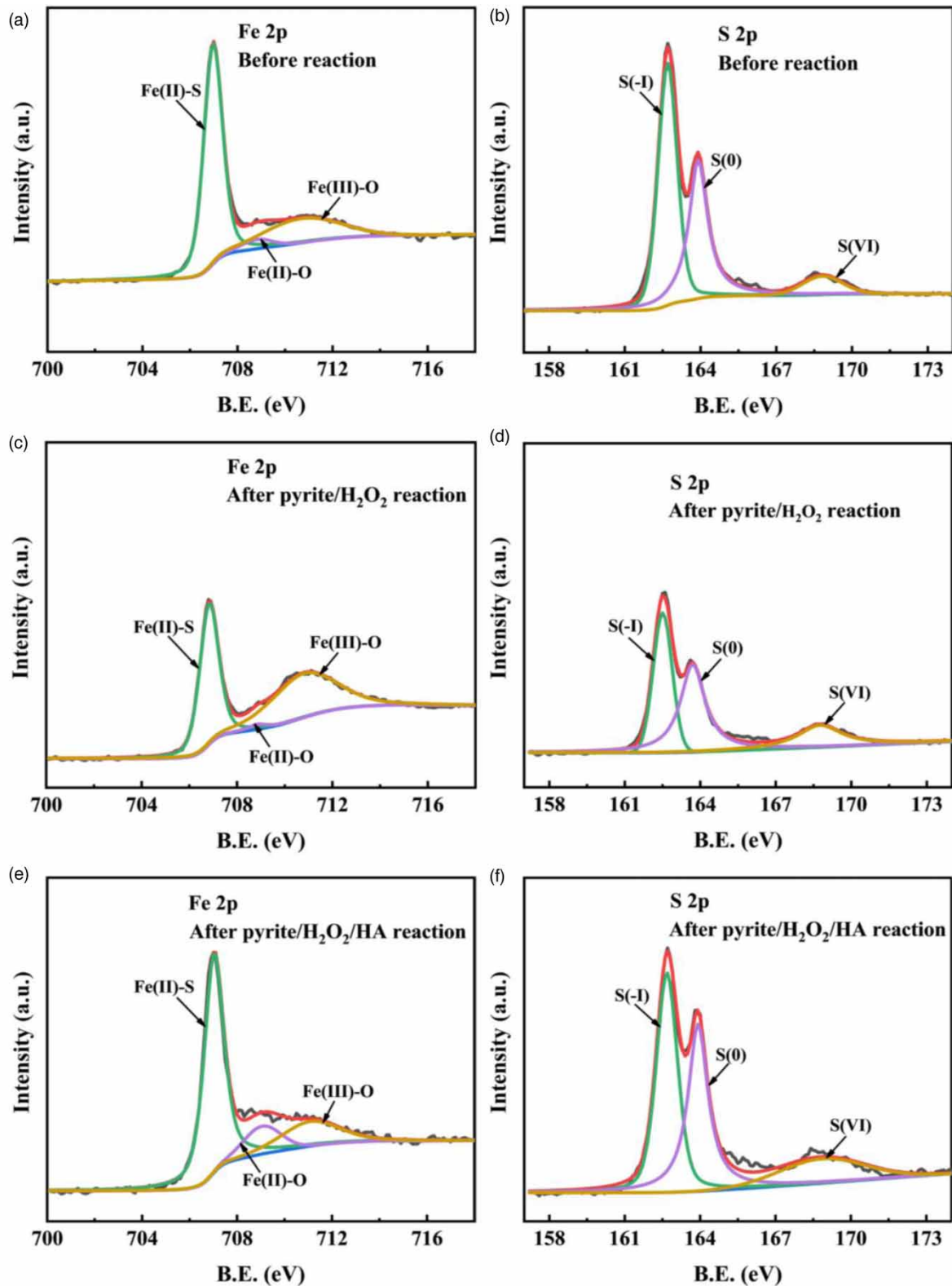
Figure 6 | (a–f) XPS spectra of Fe (2p) and S (2p) for pyrite before and after reaction in pyrite/H$_2$O$_2$ and pyrite/H$_2$O$_2$/HA systems.
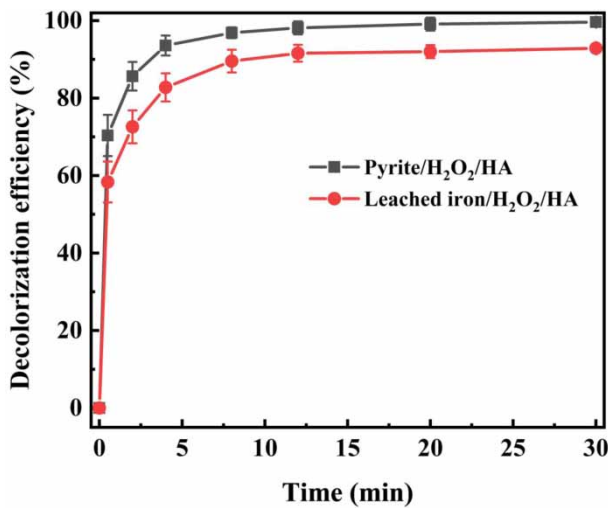
Figure 7 │ Effect of the leached iron on RhB decolorization efficiency in the pyrite/H$_2$O$_2$/HA system.

RhB decolorization, indicating that the pyrite/H$_2$O$_2$/HA system is mainly a homogeneous oxidation system.

Based on the above analysis and previous reports (Chen *et al.* 2015b; Feng *et al.* 2018; Zhou *et al.* 2018; Li *et al.* 2021), the possible reaction mechanism of RhB decolorization by the pyrite/H$_2$O$_2$/HA system is clarified by Figure 8. Fe^{2+} leached from the pyrite can react with H$_2$O$_2$ to produce •OH radicals for RhB decolorization. This procedure is promoted by HA by accelerating the Fe(II)/Fe(III) cycle via the fast oxidation of HA, and thus stimulating the decomposition of H$_2$O$_2$ to generate more •OH radicals. Meanwhile, HA can inhibit the oxidation of pyrite and enhance its continuous reactivity. In addition, HA can directly activate H$_2$O$_2$ to generate •OH radicals to degrade RhB.

Effect of HA dosing manner on RhB decolorization

As presented in Figure 5(b), the H$_2$O$_2$ consumption of the pyrite/H$_2$O$_2$/HA system was 37% higher than that of the pyrite/H$_2$O$_2$ system, while the RhB decolorization efficiency of the pyrite/H$_2$O$_2$/HA system was just about 20% higher than that of the pyrite/H$_2$O$_2$ system (Figure 2). This phenomenon may be caused by the quenching effect of HA on •OH (Equation (12)). Therefore, to investigate the quenching effect of HA on •OH and reduce it, experiments with different HA dosing manners were performed (Figure 9). A total amount of 0.8 mM HA was either dosed once at a predetermined time after the reaction start or
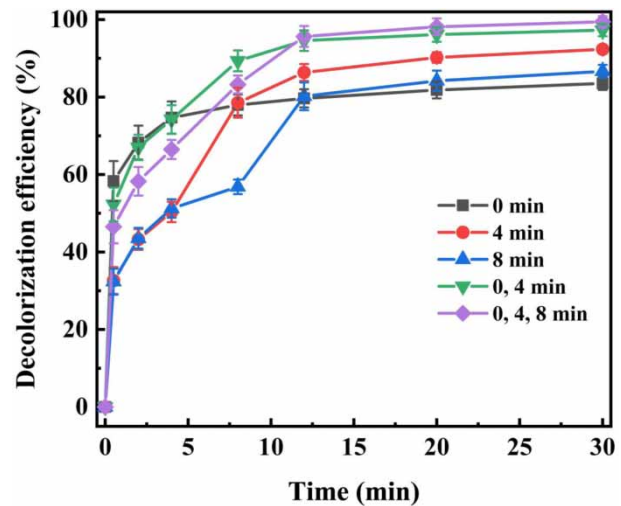

Figure 9 │ Effect of the dosing manner of HA on RhB decolorization efficiency in the pyrite/H$_2$O$_2$/HA system. [RhB]$_0$ = 100 mg L^{-1}.
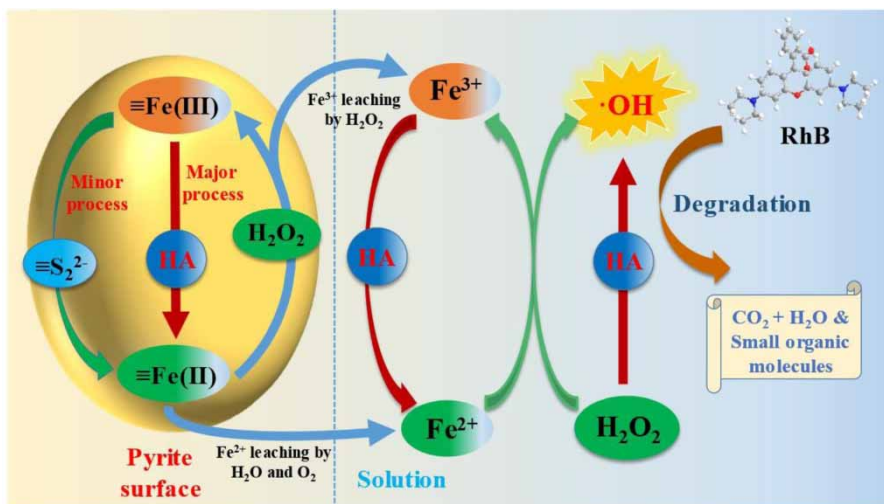

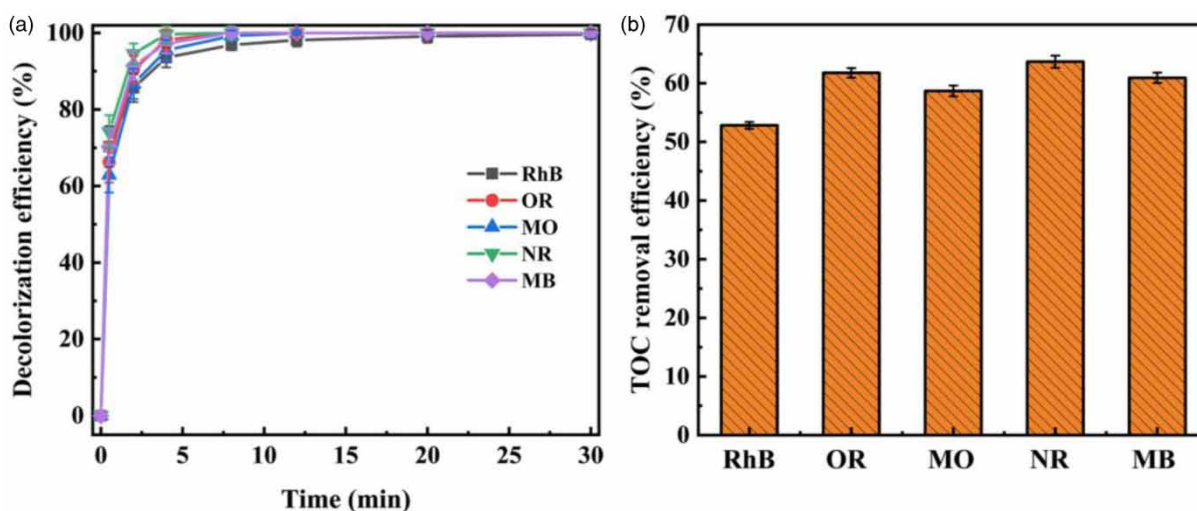**Figure 8** │ Possible reaction mechanism of RhB degradation by the pyrite/H$_2$O$_2$/HA system.

Figure 10 │ (a) Decolorization and (b) mineralization efficiencies of different dye pollutants by the pyrite/H₂O₂/HA system. [OR, MO, NR, or MB]$_0$ = 104 μM (equal to the molar concentration of 50 mg L^{-1} RhB).

dosed evenly at distinct stages into the reaction solution. Meanwhile, to simulate practical application (high concentration of dye wastewater), the concentration of 100 mg L^{-1} RhB was selected in the experiments. As shown in Figure 9, the RhB decolorization efficiency of HA dosed once at 4 min (92.3%) or 8 min (86.7%) after the reaction start was higher than that (83.5%) when dosed initially. The decolorization efficiency increases instantly when HA is dosed due to the Fe(II)/Fe(III) redox cycle promoted by the added HA. Surprisingly, more than 97% of RhB was decolorized when HA was dosed evenly at 0, 4 min and 0, 4, 8 min, respectively, which was mainly attributed the addition of HA in batches that weakened its quenching effect on ·OH. Therefore, the suitable dosing manner of HA was multiple dosing.

Decolorization and mineralization of different dye pollutants

In order to assess the applicability of the pyrite/H₂O₂/HA system, four other dye pollutants, namely OR, MO, NR and MB were treated using it. The results (Figure 10(a)) displayed that complete decolorization was achieved for four dye pollutant and RhB by the pyrite/H₂O₂/HA system only within 12 min, indicating its excellent decolorization ability in dye pollutants treatment. Moreover, the mineralization efficiencies of the four dye pollutants treated by pyrite/H₂O₂/HA system were also examined (Figure 10(b)). This showed that the mineralization efficiencies of OR, MO, NR, MB and RhB were about 61.8%, 58.7%, 63.7%, 60.9%

and 52.8%, respectively, after 30 min treatment, suggesting the excellent performance of the pyrite/H₂O₂/HA system for dye pollutant mineralization. These outcomes show that the pyrite/H₂O₂/HA system has low selectivity for dye degradation, indicating that it is a promising technique for dye pollutant treatment.

CONCLUSION

In this research, the pyrite/H₂O₂/ HA system was proposed for efficient RhB degradation in a wide pH range 3.0–10.0. Its influence factors were investigated and the optimum conditions were obtained as pyrite 0.4 g L^{-1}, H₂O₂ 1.6 mM, initial pH 4.0, HA 0.8 mM and HA added multiple times. The mechanism study showed that ·OH was the primary reactive species. HA had two key roles: one was to promote the Fe(II)/Fe(III) cycle via fast self-decomposition, and thus motivate the decomposition of H₂O₂ to produce more ·OH radicals, and finally increase the RhB decolorization; the other was to improve the continuous reactivity of pyrite by inhibiting its oxidation. Moreover, H₂O₂ was mainly activated by the leached iron ions in solution. Complete decolorization and above 52% mineralization efficiency of five dyes for 30 min treatment showed that the pyrite/H₂O₂/HA system had low selectivity for dye degradation, and it had good application prospects in organic pollutant treatment. The performance optimization of reducing agents, the toxicity evaluation of degradation intermediates,

and the application of the pyrite/H$_2$O$_2$/HA system in actual dye wastewater need further study.

DECLARATION OF COMPETING INTEREST

None.

DATA AVAILABILITY STATEMENT

All relevant data are included in the paper or its Supplementary Information.

REFERENCES

Anipsitakis, G. P. & Dionysiou, D. D. 2004 Radical generation by the interaction of transition metals with common oxidants. *Environmental Science & Technology* **38** (13), 3705–3712.

Bae, S., Kim, D. & Lee, W. 2013 Degradation of diclofenac by pyrite catalyzed Fenton oxidation. *Applied Catalysis B: Environmental* **134–135**, 93–102.

Bagal, M. V. & Gogate, P. R. 2014 Wastewater treatment using hybrid treatment schemes based on cavitation and Fenton chemistry: a review. *Ultrasonics Sonochemistry* **21** (1), 1–14.

Banazadeh, A., Salimi, H., Khaleghi, M. & Shafiei-Haghighi, S. 2016 Highly efficient degradation of hazardous dyes in aqueous phase by supported palladium nanocatalyst—A green approach. *Journal of Environmental Chemical Engineering* **4** (2), 2178–2186.

Brillas, E. & Martínez-Huitle, C. A. 2015 Decontamination of wastewaters containing synthetic organic dyes by electrochemical methods. An updated review. *Applied Catalysis B: Environmental* **166–167**, 603–643.

Cai, Y., Pan, Y., Xue, J., Sun, Q., Su, G. & Li, X. 2009 Comparative XPS study between experimentally and naturally weathered pyrites. *Applied Surface Science* **255** (21), 8750–8760.

Chen, L., Ma, J., Li, X., Zhang, J., Fang, J., Guan, Y. & Xie, P. 2011 Strong enhancement on Fenton oxidation by addition of hydroxylamine to accelerate the ferric and ferrous iron cycles. *Environmental Science & Technology* **45** (9), 3925–3930.

Chen, H., Zhang, Z., Yang, Z., Yang, Q., Li, B. & Bai, Z. 2015a Heterogeneous Fenton-like catalytic degradation of 2,4-dichlorophenoxyacetic acid in water with FeS. *Chemical Engineering Journal* **273**, 481–489.

Chen, L., Li, X., Zhang, J., Fang, J., Huang, Y., Wang, P. & Ma, J. 2015b Production of hydroxyl radical via the activation of hydrogen peroxide by hydroxylamine. *Environmental Science & Technology* **49** (17), 10373–10379.

Diao, Z., Liu, J., Hu, Y., Kong, L., Jiang, D. & Xu, X. 2017 Comparative study of Rhodamine B degradation by the systems pyrite/H$_2$O$_2$ and pyrite/persulfate: reactivity,

stability, products and mechanism. *Separation and Purification Technology* **184**, 374–383.

Eisenberg, G. 1943 Colorimetric determination of hydrogen peroxide. *Industrial & Engineering Chemistry-Analytical Edition* **15** (5), 327–328.

Feng, Y., Li, H., Lin, L., Kong, L., Li, X., Wu, D., Zhao, H. & Shih, K. 2018 Degradation of 1,4-dioxane via controlled generation of radicals by pyrite-activated oxidants: synergistic effects, role of disulfides, and activation sites. *Chemical Engineering Journal* **336**, 416–426.

Frear, D. S. & Burrell, R. C. 1955 Spectrophotometric method for determining hydroxylamine reductase activity in higher plants. *Analytical Chemistry* **27** (10), 1664–1665.

Gu, X., Heaney, P. J., Reis, F. & Brantley, S. L. 2020 Deep abiotic weathering of pyrite. *Science* **370** (6515), 1–8.

He, D. Q., Zhang, Y. J., Pei, D. N., Huang, G. X., Liu, C., Li, J. & Yu, H. Q. 2020 Degradation of benzoic acid in an advanced oxidation process: the effects of reducing agents. *Journal of Hazardous Materials* **382**, 121090.

He, P., Zhu, J., Chen, Y., Chen, F., Zhu, J., Liu, M., Zhang, K. & Gan, M. 2021 Pyrite-activated persulfate for simultaneous 2,4-DCP oxidation and Cr(VI) reduction. *Chemical Engineering Journal* **406**, 126758.

Hickerson, R. P., Watkins-Sims, C. D., Burrows, C. J., Atkins, J. F., Gesteland, R. F. & Felden, B. 1998 A nickel complex cleaves uridine in folded RNA structures: application to *E. coli* tmRNA and related engineered molecules. *Journal of Molecular Biology* **279** (3), 577–587.

Hou, X., Huang, X., Jia, F., Ai, Z., Zhao, J. & Zhang, L. 2017 Hydroxylamine promoted goethite surface Fenton degradation of organic pollutants. *Environmental Science & Technology* **51** (9), 5118–5126.

Hughes, M. N., Nicklin, H. G. & Shrimanker, K. 1971 Autoxidation of hydroxylamine in alkaline solutions. Part II. Kinetics. The acid dissociation constant of hydroxylamine. *Journal of the Chemical Society A: Inorganic, Physical, Theoretical* **1971**, 3485–3487.

Javaid, R. & Qazi, U. Y. 2019 Catalytic oxidation process for the degradation of synthetic dyes: an overview. *International Journal of Environmental Research and Public Health* **16** (11), 2066–2093.

Li, J., Wan, Y., Li, Y., Yao, G. & Lai, B. 2019a Surface Fe(III)/Fe(II) cycle promoted the degradation of atrazine by peroxymonosulfate activation in the presence of hydroxylamine. *Applied Catalysis B: Environmental* **256**, 117782.

Li, Y., Zhao, X., Yan, Y., Yan, J., Pan, Y., Zhang, Y. & Lai, B. 2019b Enhanced sulfamethoxazole degradation by peroxymonosulfate activation with sulfide-modified microscale zero-valent iron (S-mFe0): performance, mechanisms, and the role of sulfur species. *Chemical Engineering Journal* **376**, 121302.

Li, T., Abdelhaleem, A., Chu, W. & Xu, W. 2021 Efficient activation of oxone by pyrite for the degradation of propanil: kinetics and degradation pathway. *Journal of Hazardous Materials* **403**, 123930.

Luo, H., Zhao, Y., He, D., Ji, Q., Cheng, Y., Zhang, D. & Pan, X. 2019 Hydroxylamine-facilitated degradation of rhodamine B (RhB)

and p-nitrophenol (PNP) as catalyzed by Fe@Fe$_2$O$_3$ core-shell nanowires. *Journal of Molecular Liquids* **282**, 13–22.

Mahalingam, S., Ramasamy, J. & Ahn, Y.-H. 2017 Enhanced photocatalytic degradation of synthetic dyes and industrial dye wastewater by hydrothermally synthesized G–CuO–Co$_3$O$_4$ hybrid nanocomposites under visible light irradiation. *Journal of Cluster Science* **29** (2), 235–250.

Neta, P., Huie, R. E. & Ross, A. B. 1988 Rate constants for reactions of inorganic radicals in aqueous solution. *Journal of Physical and Chemical Reference Data* **17** (3), 1027–1284.

Oral, O. & Kantar, C. 2019 Diclofenac removal by pyrite-Fenton process: performance in batch and fixed-bed continuous flow systems. *Science of The Total Environment* **664**, 817–823.

Robinson, R. A. & Bower, V. E. 1961 The ionization constant of hydroxylamine. *Journal of Physical Chemistry* **65** (7), 1279–1280.

Stemmler, A. J. & Burrows, C. J. 2001 Guanine versus deoxyribose damage in DNA oxidation mediated by vanadium(IV) and vanadium(V) complexes. *Journal of Biological Inorganic Chemistry* **6** (1), 100–106.

Sun, H., He, F. & Choi, W. 2020a Production of reactive oxygen species by the reaction of periodate and hydroxylamine for rapid removal of organic pollutants and waterborne bacteria. *Environmental Science & Technology* **54** (10), 6427–6437.

Sun, X., Liu, J., Ji, L., Wang, G., Zhao, S., Yoon, J. Y. & Chen, S. 2020b A review on hydrodynamic cavitation disinfection: the current state of knowledge. *Science of the Total Environment* **737**, 139606.

Sun, X., Xuan, X., Song, Y., Jia, X., Ji, L., Zhao, S., Yong Yoon, J., Chen, S., Liu, J. & Wang, G. 2021 Experimental and numerical studies on the cavitation in an advanced rotational hydrodynamic cavitation reactor for water treatment. *Ultrasonics Sonochemistry* **70**, 105311.

Todd, E. C., Sherman, D. M. & Purton, J. A. 2003 Surface oxidation of pyrite under ambient atmospheric and aqueous (pH = 2 to 10) conditions: electronic structure and mineralogy from X-ray absorption spectroscopy. *Geochimica et Cosmochimica Acta* **67** (5), 881–893.

Wang, N., Zheng, T., Zhang, G. & Wang, P. 2016 A review on Fenton-like processes for organic wastewater treatment. *Journal of Environmental Chemical Engineering* **4** (1), 762–787.

Wang, S., Jia, Y., Song, L. & Zhang, H. 2018 Decolorization and mineralization of Rhodamine B in aqueous solution with a

triple system of cerium(IV)/H$_2$O$_2$/hydroxylamine. *ACS Omega* **3** (12), 18456–18465.

Ye, Y., Shan, C., Zhang, X., Liu, H., Wang, D., Lv, L. & Pan, B. 2018 Water decontamination from Cr(III)-organic complexes based on pyrite/H$_2$O$_2$: performance, mechanism, and validation. *Environmental Science & Technology* **52** (18), 10657–10664.

Yuan, S., Gou, N., Alshawabkeh, A. N. & Gu, A. Z. 2013 Efficient degradation of contaminants of emerging concerns by a new electro-Fenton process with Ti/MMO cathode. *Chemosphere* **93** (11), 2796–2804.

Zhang, Y., Zhang, K., Dai, C., Zhou, X. & Si, H. 2014 An enhanced Fenton reaction catalyzed by natural heterogeneous pyrite for nitrobenzene degradation in an aqueous solution. *Chemical Engineering Journal* **244**, 438–445.

Zhao, L., Chen, Y., Liu, Y., Luo, C. & Wu, D. 2017 Enhanced degradation of chloramphenicol at alkaline conditions by S(-II) assisted heterogeneous Fenton-like reactions using pyrite. *Chemosphere* **188**, 557–566.

Zhao, Z., Pan, S., Ye, Y., Zhang, X. & Pan, B. 2020 FeS$_2$/H$_2$O$_2$ mediated water decontamination from p-arsanilic acid via coupling oxidation, adsorption and coagulation: performance and mechanism. *Chemical Engineering Journal* **381**, 122667.

Zhou, Y., Wang, X., Zhu, C., Dionysiou, D. D., Zhao, G., Fang, G. & Zhou, D. 2018 New insight into the mechanism of peroxymonosulfate activation by sulfur-containing minerals: role of sulfur conversion in sulfate radical generation. *Water Research* **142**, 208–216.

Zhou, Y., Huang, M., Wang, X., Gao, J., Fang, G. & Zhou, D. 2020 Efficient transformation of diethyl phthalate using calcium peroxide activated by pyrite. *Chemosphere* **253**, 126662.

Zhu, Y., Zhu, R., Xi, Y., Zhu, J., Zhu, G. & He, H. 2019 Strategies for enhancing the heterogeneous Fenton catalytic reactivity: a review. *Applied Catalysis B: Environmental* **255**, 117739.

Zhu, X., Li, J., Xie, B., Feng, D. & Li, Y. 2020 Accelerating effects of biochar for pyrite-catalyzed Fenton-like oxidation of herbicide 2,4-D. *Chemical Engineering Journal* **391**, 123605.

Zou, J., Ma, J., Chen, L., Li, X., Guan, Y., Xie, P. & Pan, C. 2013 Rapid acceleration of ferrous iron/peroxymonosulfate oxidation of organic pollutants by promoting Fe(III)/Fe(II) cycle with hydroxylamine. *Environmental Science & Technology* **47** (20), 11685–11691.